



Improved NO₂ sensing performance of nanostructured Zn doped SnO₂ thin films

R. H. Bari, S. B. Patil*

^{1*}Nanomaterials Research Laboratory, Department of Physics, G. D. M. Arts, K. R. N. Commerce and M.D. Science College, Jamner 424 206, Maharashtra, India.

Abstract : Gas sensor based on nanostructured pure SnO₂ and Zn doped SnO₂ thin films has been synthesized by using spray pyrolysis technique and evaluated for NO₂ gas sensing (Gas response=S ~ 1480) at operating temperature 150 °C with 100 ppm. Sensor structure showed the short response and recovery times 3 and 10 s, respectively. The nanostructured pure SnO₂ and Zn doped SnO₂ thin films were used as potential gas sensing material for their stability in thermal and chemical atmospheres. Structural, surface morphology, elemental composition, microstructural, optical and NO₂ gas sensing performance of different vol % of Zn (3-7%) were studied and reported. Prepared thin films were characterized by different analytical techniques. The results are discussed and interpreted.

Keywords : Spray pyrolysis techniques, Nanostructured Zn doped SnO₂, NO₂ sensor, Gas response.

1.0 Introduction

In the recent years, nanostructure thin films of Zn, In, Sn and Cd oxides have received considerable attention, mainly due to their important potential applications, which include photovoltaic solar cells [1,2], gas sensors [3,4], transparent electrodes [5] and other optoelectronic devices [6].

Tin dioxide is an n-type wide band gap semiconductor with a very low densification rate due to its high surface diffusion at low temperatures and high SnO₂ partial vapour pressure at sintering temperatures [7]. Pianaro et al. reported that doping with CoO and Nb₂O₅ drastically improve the sinterability of SnO₂ [8]. In order to achieve the maximum gas response the grain size must be smaller than two times of depleting layer [9]. The role of the oxygen vacancies generated by these transition metal oxides as the driving force for densification has been thoroughly treated in the literature [10–12]. Wagh and Patil et al reported the RuO₂ and Fe₂O₃ surface modified SnO₂ thick film for LPG gas sensor [13,14].

Semiconductor metal oxide gas sensors improve their gas response, selectivity, response and recovery time due to nanocrystalline nature of the material associated, which is the most attractive quality of nanomaterials. Basically the improvements are because of the high surface area to volume ratio and smaller crystallite size compared to conventional microcrystalline materials [15].

In present work we have modified the surface of SnO₂ thin films using Zn catalyst to improve gas sensing performance. Therefore, spray pyrolysis technique was employed to prepare pure SnO₂ and Zn doped SnO₂ thin films because the technique is simple and involves low cost equipments and raw materials. The technique involves a simple technology in which an ionic solution (containing the constituent elements of a compound in the form of soluble salts) is sprayed over heated substrates [16]. By this method, dopants can be easily introduced into the matrix of the film by using appropriate precursors [17]. Additives or dopants enhance the properties of the sensors, such as gas response, selectivity, lowering the operating temperature, response and recovery time etc. [18-20]

2. Experimental

2.1.Preparation of solution

The precursor solution used was of 0.05 M concentration of high purity tin (II) chloride dehydrate ($\text{SnCl}_2 \cdot 2\text{H}_2\text{O}$) Made Purified Merck) prepared in deionized water. Zinc acetate dyhydrate ($\text{Zn} \cdot 2\text{H}_2\text{O}$ (CH_3COO)₂) Purified Merck) was used as the source of dopant. The dopant volume (% Zn) was varied from 3 to 7% as presented in Table 1.1

Table 1: Preparation of solution.

Sample	Dopping level	Solution in (ml)		Total
		Tin (II) chloride dehydrate	Zinc acetate dyhydrate	
1	0	100	00	100
2	3	97	3	100
3	5	95	5	100
4	7	93	7	100

2.2 Preparation of pure nanostructured SnO_2 thin films

The spraying solution was prepared by mixing the appropriate volumes of 0.05 M Tin (II) chloride dehydrate ($\text{SnCl}_2 \cdot 2\text{H}_2\text{O}$), Purified Merck) in de-ionized water as a precursor. The SnO_2 films were deposited at spraying time of 30 min was obtained and referred to pure SnO_2 . The optimized values of important preparative parameters are shown in table 2.

2.3 Preparation of nanostructured Zn-modified SnO_2 thin films

The atomization of the solution into a spray of fine droplets was carried out by a spray pyrolysis technique. Thus the modified films of 30 min spraying time with different dopant volume (% Zn): 3, 5 and 7 were obtained and referred to K1, K2, and K3 respectively. Process parameters for the spray deposition of nanostructure pure SnO_2 and Zn doped SnO_2 thin films were tabulated in Table 2.

2.4 Optimized parameters

Table 2: Process parameters for the spray deposition of nanostructure pure SnO_2 and Zn doped SnO_2 thin films.

Spray parameter	Optimum value / item
Nozzle	Glass
Nozzle to substrate distance	30 cm
Tin (II) chloride dehydrate solution concentration	0.05M
Zinc acetate dehydrate solution concentration	0.05M
Volume % of Zn	3, 5, and 7
Spray deposition time	30 min.
Solvent	Deionised water
Solution flow rate	7 ml/ min.
Carrier gas	Compressed air
Substrate temperature	250 °C

2.5 Post preparative treatment (annealing)

As the prepared nanostructured pure SnO_2 and Zn doped SnO_2 thin film samples were annealed at 500 °C for 1 hour.

2.6 Details of gas sensing system

The gas sensing performance were carried out using a static gas chamber to sense NO_2 gas in air ambient and the experimental set up is described elsewhere [21]. The nanostructured pure SnO_2 and Zn doped

SnO_2 thin films were used as the sensing elements. Cr-Al thermocouple is mounted to measure the temperature. The output of thermocouple is connected to temperature indicator. Gas inlet valve fitted at one of the ports of the base plate. The air was allowed to pass into the glass chamber before start of every new gas exposure cycle. Gas concentration (100 ppm) inside the static system is achieved by injecting a known volume of test gas in gas injecting syringe. The conductance of the sensor in dry air was measured by means of conventional circuitary by applying constant voltage (5V) and measuring the current by picoammeter. The conductance was measured both in the presence and absence of test gas.

The gas response (S) is defined as the ratio of change in conductance in gas to air to the original conductance in air.

$$S = \frac{G_g - G_a}{G_a} \quad \dots \quad (1)$$

Where, G_a = the conductance of the sensor in air

G_g = the conductance on exposure of a target gas.

3. Characterizations

The crystal structure of films was analyzed with X-ray diffractometer (Miniflex Model, Rigaku, Japan, Advanced D8) by using Cu-K α lines ($\lambda = 1.542\text{\AA}$). Surface morphology was examined by JEOL model JSM-6400 scanning electron microscope (SEM) coupled with EDAX. Microstructure property was studied using transmission electron microscopy (TEM, TECNAI G²20-TWIN FET, NETHERLAND: CM 200 Philips 200 kV HT). Optical band gap studies were conducted using UV-VIS absorption spectroscopy (Shimadzu 2450 UV-VIS). Measurement of thermoelectrical power was conducted using TEP set up (Made-Pushpa agency-Hyderabad). Electrical conductivity and gas sensing properties were checked using a static gas sensing system for different conventional gases.

4. Results and Discussion

4.1. Structural studies using XRD

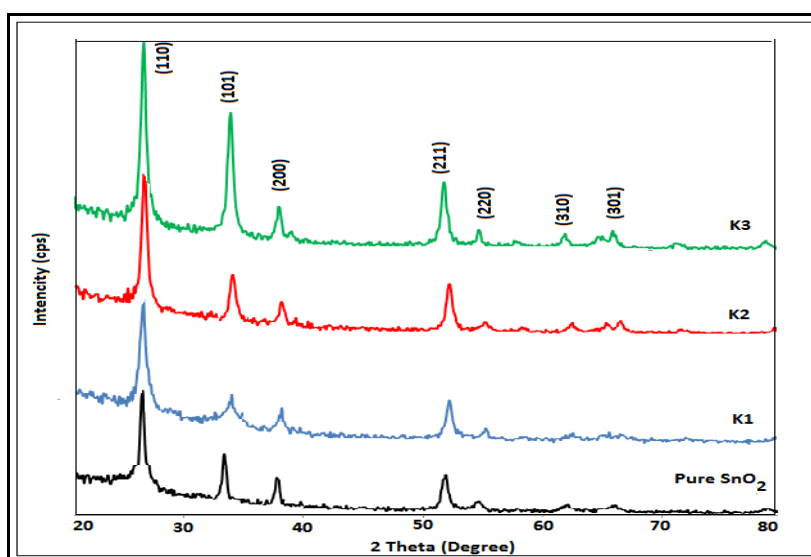


Figure 1: X-ray diffractogram : pure SnO_2 and Zn doped SnO_2 (K1,K2 and K3) nanostructured thin film.

Fig. 1 shows the X-ray diffractogram of pure SnO_2 and Zn doped SnO_2 . The observed peaks are matching well with JCPDS reported data of SnO_2 (JCPDS data card No. 21-1250). The average crystallite size was obtained from Scherrer's formula.

$$D = \frac{0.9\lambda}{\beta \cos\theta} \quad \dots \quad (2)$$

Where, D = Average crystallite size

λ = X-ray wavelength (1.5418 Å)

β = FWHM of the peak

θ = Diffraction peak position.

The broad peaks of the XRD pattern corresponding to SnO₂ material are observed to be nanocrystalline in nature. No peak corresponding to Zn was observed. It may be due to its very small at % in the thin film. The average crystallite size was estimated in table 4.

4.2 Morphological studies using SEM

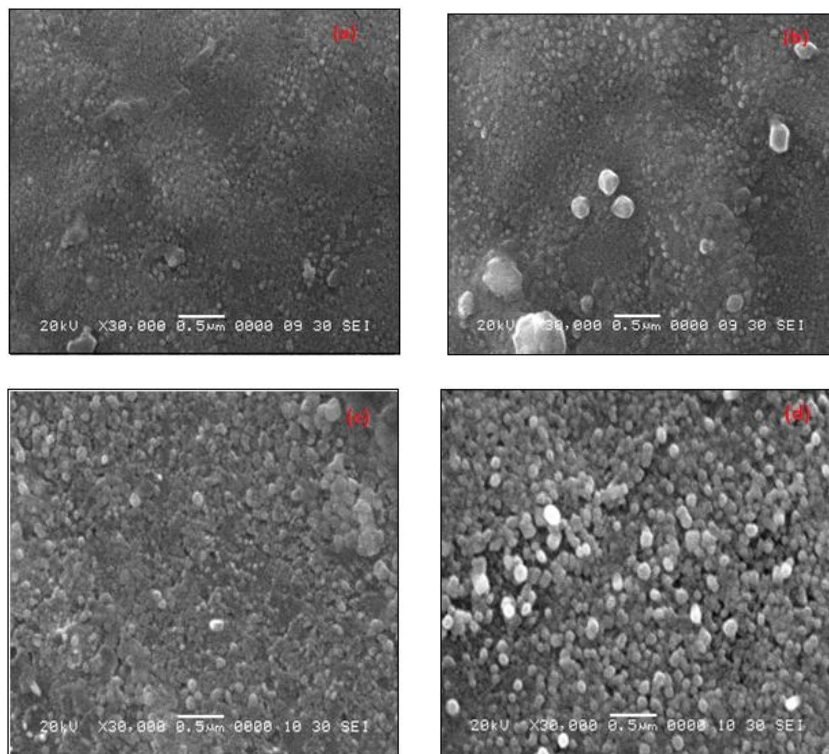


Figure 2 (a-d): SEM images of prepared pure SnO₂ and Zn doped SnO₂ thin film

The surface morphology of the prepared film was analyzed using a scanning electron microscope. SEM image of pure SnO₂ and Zn doped SnO₂ (K1-K3) thin film samples is represented in Fig. 2. Scanning electron microscope resolve nanoparticles associated with the film even at very high magnification of “30E+3”. It may be due to very small nanocrystalline particles associated with the thin film. Spherical grains with different shapes were observed from SEM images. Grain size estimated form SEM images were tabulated in table 4.

4.3 Elemental compositional studies using EDAX

Table 3 shows the elemental composition of the films determined by EDAX.

Table 3: Elemental compositions of thin films.

Element	Observed							
	mass %	at %	mass %	at %	mass %	at %	mass %	at %
Sn	74.97	28.76	29.57	29.26	36.73	30.48	50.91	35.49
O	25.03	71.24	56.78	70.66	35.42	69.40	27.44	64.33
Zn	-	-	13.65	00.08	27.85	00.12	21.65	00.18
Total	100.00	100.00	100.00	100.00	100.00	100.00	100.00	100.00

The quantitative elemental composition of the pure and Zn-modified SnO₂ thin films was analysed using an energy dispersive spectrometer and atomic percentage (at %) of Sn, O, Zn are represented in Table 3. The stoichiometric at% of Sn and O in SnO₂ is 66.66 and 33.33, respectively. Atomic percentage (at %) of Sn

and O in each sample was observed to be the nonstoichiometric proportion and all samples were observed to be oxygen deficient. It is clear from Table 3, that as at% of oxygen goes on decreasing with the increasing at% of Zn in SnO₂.

4.4 Microstructural studies using TEM

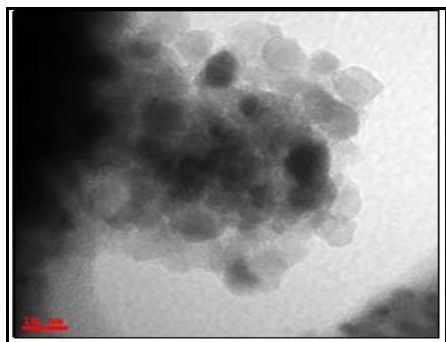


Figure 3: TEM images of the nanostructured of most sensitive thin sample =K2

The microstructure image of the Zn doped SnO₂ thin films sample is shown in Fig. 3. These TEM images show clear showing nearly spherical shaped crystallites having size of ~17 nm.

4.5 Optical band gap studies using UV spectroscopy

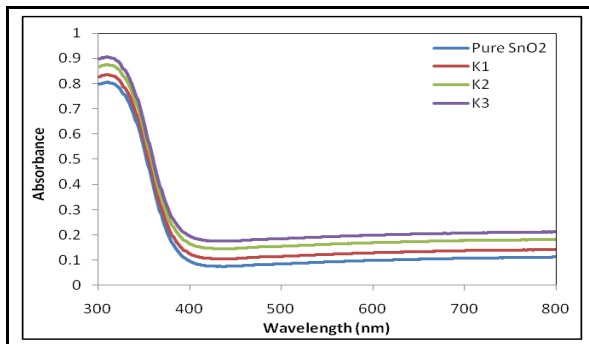


Figure 4: The variation of relative absorbance with wavelength (nm) for nanostructured pure SnO₂ and Zn doped SnO₂ (K1-K3) thin films.

Optical absorption studies of pure SnO₂ and Zn doped SnO₂ thin films were conducted in the wavelength (λ) range 300-800 nm at room temperature. The variation of absorbance with wavelength (λ) as shown in Fig. 4. The band gap energies of the samples were calculated from the absorption edges of the spectra. The slope drawn from the start of an absorption edge (the onset of absorbance) and horizontal tangent had drawn on absorption minimum and intercepted each other at some point. The vertical line drawn from this point on wavelength axis gave the absorption edge wavelength.

This value of λ (nm) was then used in the following relation to know band gap energy:

$$Eg = h c / \lambda = (1240) / \lambda \text{ (nm)} \text{ eV} \quad \dots \dots \dots (3)$$

Optical band gap energy was found to be 3.61 to 3.90 eV.

5. Electrical properties of the pure and modified sensor

5.1 Thermoelectric power (TEP) measurements

The n-type semiconductivity of pure and Zn-modified SnO₂ thin films were confirmed by measuring thermo-electromotive power of thin film sensor.

5.2 I-V characteristics

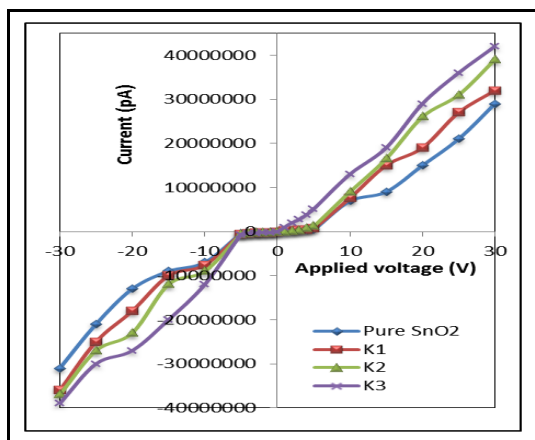


Figure 5: I-V characteristics of nanostructured thin film sensors.

Fig. 5 shows the I-V characteristics of nanocrystalline pure and Zn-modified SnO_2 thin films. It is clear from Fig. 5 that the I-V characteristics of pure and nanostructured Zn modified SnO_2 thin films are observed to symmetrical in nature indicating the ohmic contact.

5.3 Electrical conductivity

Figure 6 shows the electrical conductivity of the nanocrystalline pure and Zn modified SnO_2 thin films. Conductivity of each sample is increasing with increase of temperature. This increase in conductivity with increase of temperature is attributed to improvement of charge density and semiconducting nature of the films.

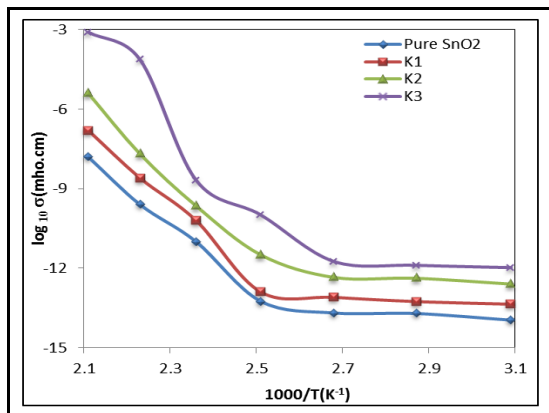


Figure 6: Electrical conductivity of nanostructured thin film sensors.

Electrical conductivity was calculated using the relation:

$$\sigma = \sigma_0 \exp(-\Delta E/kT) \quad \dots \quad (4)$$

Where, σ = conductivity

σ_0 = conductivity constant

k = Boltzmann constant

T = Temperature

The activation energy was calculated from the slope of the graph of $\log(\sigma)$ against $1000/T (\text{K}^{-1})$ for particular samples. Activation energy was tabulated in table 4.

Table 4: Measurement of Zn content, crystallite size, grain size, optical band gap energy and activation energy

Sample	Zn %	Crystalline size from XRD(nm)	Grain size from SEM(nm)	Optical band gap energy eV	Activation energy $\triangle E$ eV
Pure SnO ₂	-	19	23	3.61	0.35
K1	3	26	27	3.74	0.31
K2	5	31	29	3.87	0.29
K3	7	33	31	3.90	0.26

It is also clear from table 4, that crystalline size, grain sizes and optical band gap energy were goes on increasing with increase in Zn content in the SnO₂. Optical band gap energy was observed to be large as compared to reported value 3.6 eV. There is a large increase in observed band gap energies of the as prepared films. It means there is large change in optical properties of the films. Large change (increase) in band gap energy is the evidence of nanocrystalline nature the as prepared films. Another reason could be the improving crystallinity with increasing grain size. Table 4 represents the variation of activation energy with Zn % in SnO₂ thin films. The activation energy decreases with Zn %. The activation energy of the pure SnO₂ sample was larger than those of Zn doped SnO₂ thin film samples. The activation energy was observed to be the smallest for the sample modified with the largest concentration of Zn [22].

6. Sensing performance of Zn-modified thin film sensors

6.1 Gas response with operating temperature

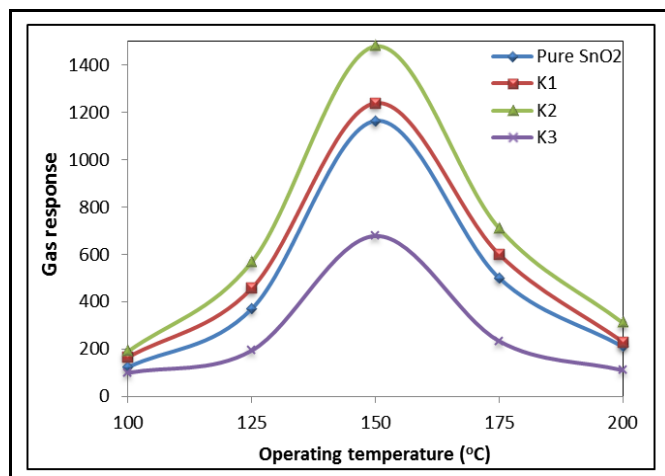
**Figure 7: Variation of response with operating temperature of Zn modified SnO₂ thin film.**

Fig.7 depicts the variation of gas response with operating temperature of nanostructured Zn modified SnO₂ thin film to 100 ppm NO₂. It is clear from Fig. 7 that the gas response increases with operating temperature, reaches to maximum at 150 °C and falls with further increase in operating temperature. It is also clear from figure that the NO₂ response goes on increasing with increase in % Zn in SnO₂ and reaches to maximum at (vol) 5% Zn (film K2) and decrease further with increase in % Zn.

6.2 Selectivity

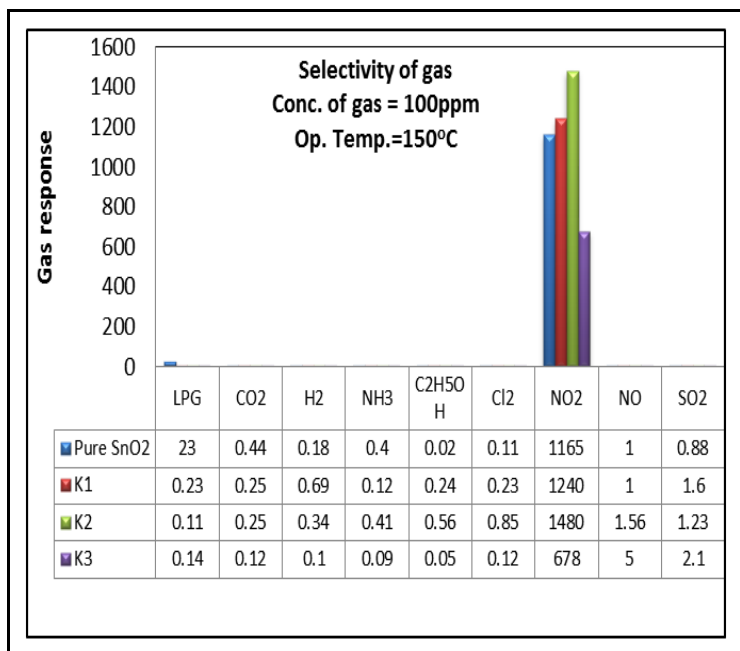


Figure 8: Selectivity profile of nanostructured pure and Zn modified SnO₂ against various gases

Fig. 8 shows the variation of gas responses of nanostructured pure and Zn modified SnO₂ to thin films to NO₂ (100 ppm) among the mixture of gases. It is clear from the figure that the nanostructured Zn modified SnO₂ samples show the enhanced and selective response to NO₂ at 150 °C among all other gases. The film surface chemistry would have been favorable to oxidize the NO₂ easily than other gases, giving larger response to NO₂ and smaller to others.

6.3 Response and recovery time with concentration of gas (ppm)

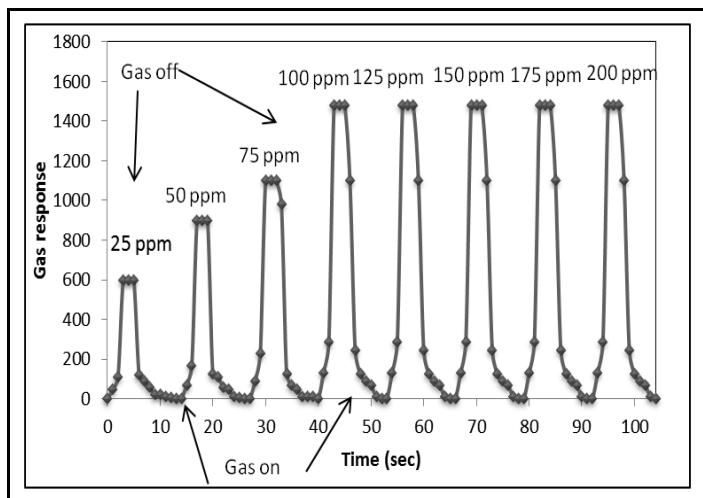


Figure 9: Response and recovery time of (Most sensitive=K2) thin film sensor.

It is clear from the Fig. 9 that, the gas response goes on increasing with gas concentration up to 100 ppm. The rate of increase in response was relatively larger up to 100 ppm and saturated beyond 100 ppm. The excess gas would form multimolecular layer on the film surface and the part of gas amount would be idle and unable to interact with sensor surfaces. Hence response would saturate further. The 90% response and recovery levels were attained within 3 and 10 seconds respectively. The very short response and recovery times are the important features of the nanostructured Zn modified SnO₂ thin film sensor. The negligible quantity of the surface reaction products and their high volatility may be reason of the quick response to hydrogen and fast recovery to its initial chemical status.

Table 5. Literature survey on SnO₂ and surface modified Zn doped SnO₂ based NO₂ gas sensors.

Sr. No.	Material	Method	Temp. (°C)	Gas con. (ppm)/ (ppb)	NO ₂ gas response / sensitivity	Response and recovery time	References
1	Zn-SnO ₂	Spray method	150	100	1480	3 sec/ 10 sec	Present work (Sample K2)
2	SnO ₂	Electrophoretic deposition	105	13.7	61	90 sec / 10 sec	23
3	Au-SnO ₂	Chemical route	300	2000	3.5	20min/ 50 min	24
4	WO ₃ /Au-SnO ₂	Screen Printing	-	10	1	2min/ 3 min	25
5	WO ₃ -SnO ₂	Powder mixing (Ball milling)	300	5	6.5	-	26
6	Ru -SnO ₂	Evaporation	1000	200	3500	100 sec/ 300 sec	27
7	Fe ₂ O ₃ - SnO ₂	Wet Chemical	170	1000	170	5min/ 40min	28
8	ZnO -SnO ₂	Pulse Laser Deposition	180	100	3.2	4min/ 8 min	29
9	ZnO -SnO ₂	Two-Step Vapor Growth	300	10	12.3	5 sec/ 12 sec	30

Table 5 presents comparison of NO₂ response with reported different sensor and sensor prepared in present investigation [23–30]. It is clear that response of sensor reported in the present work is extremely high as compared to previous reported sensors.

7. Discussion

7.1 Gas sensing mechanism of NO₂ sensor

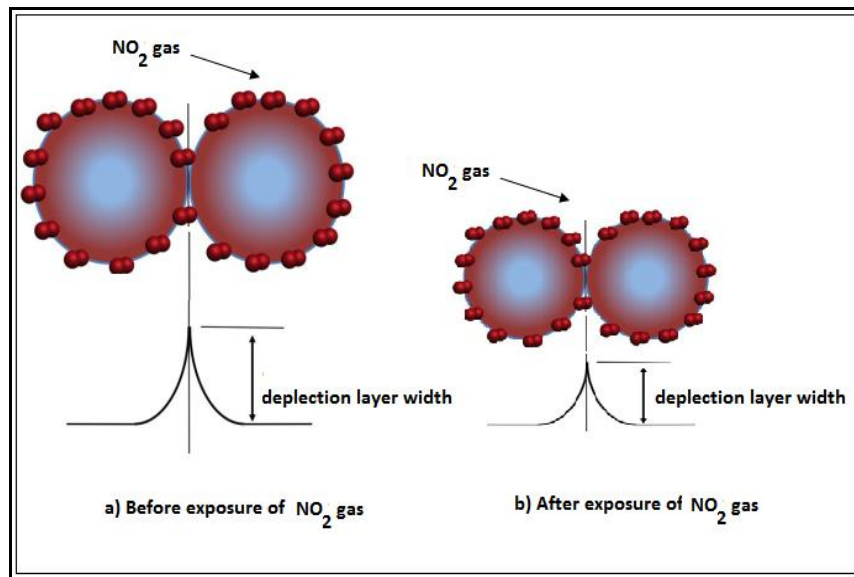
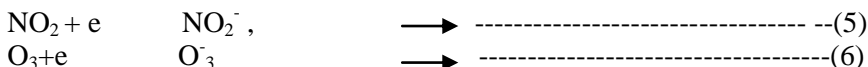
**Figure 10:** NO₂ gas sensing mechanism of nanostructured thin film sensor

Fig. 10 shows the gas sensing mechanism for NO₂ sensor. Before exposure of the gas width of depletion layer is large, when the gas is exposed on the surface of the sensor width of depletion was observed to be reduced [31]. The width of depletion layer is proportional to the surface coverage of oxygen species, the reaction to reducing gases thus decrease energy barriers between adjacent particles and increase the effective conduction channel in the semiconductors, which result in overall increase in device conductivity (maximum gas response).

Fig. 10 shows the situation when the metal oxide is exposed to oxidizing gases, such as NO₂. The oxidizing gas molecules play roles similar to oxygen species that trapped electron from metal oxide semiconductors are explained by below reaction:



8. Conclusions

1. Spray pyrolysis technique is simple, inexpensive was successfully used for preparation of pure nanostructured SnO₂ and Zn modified SnO₂ thin films.
2. It may be useful for the large scale production of nanostructured thin films.
3. The crystallite sizes were observed to be in the range of ~19 nm to 33 nm.
4. It was confirmed from SEM analysis that the grains were nearly spherical in nature with a size distribution in the range of ~23 to 31 nm.
5. EDAX results shows that prepared thin films were nonstoichiometric in nature.
6. TEM analysis confirms that the formation of nanocrystalline thin films with grain size ~ 10 nm.
7. The band gap energy calculated from absorption spectra was observed to be varying from 3.61 to 3.3.74 eV.
8. The crystallite size, grain size and band gap energy was observed to be increased with increase of vol % (3-7) of Zn in SnO₂ while activation energy decreases.
9. Zn (5 vol%) doped SnO₂ thin film showed higher gas response to NO₂ as compared to pure SnO₂ thin film. Doping of Zn into SnO₂ helped to enhance the response, selectivity towards NO₂ gas at 150 °C.
10. The sensor showed quick response (3 s) and fast recovery (10 s).
11. Overall it was summarized that, doping improved selectivity, response and recovery time of the sensor.

Acknowledgements

The authors are thankful to the University Grants Commission, New Delhi for providing financial support. Thanks to Principal, G. D. M. Arts, K. R. N. Commerce and M.D. Science College, Jamner, for providing laboratory facilities for this work.

References

1. Champness C.H., Chan C.H., Optimization of CdO layer in a Se-CdO photovoltaic cell. Sol. Ener. Mater. Sol. Cells, 1995, 37, 72-75.
2. Ramakrishna Reddy K.T., Ravani C. S., Miles R.W., Characterisation of CdO thin films deposited by activated reactive evaporation, J. Cryst. Growth, 1998, 184, 1031-1034.
3. Patil L.A., Shinde M.D., Bari A.R., Deo V.V., Highly sensitive and quickly responding ultrasonically sprayed nanostructured SnO₂ thin films for hydrogen gas sensing, Sensors and Actuators B, 2009, 143, 270-277.
4. Patil G. E., Kajale D. D., Chavan D. N., Pawar N. K., Gayakwad V. B., Jain G. H., Spray pyrolysed polycrystalline tin oxide thin films as hydrogen sensor, Sensors & Transducers, 2010, 12, 70-79.
5. Rout C.S., Kulkarni G.U., Rao C. N., Room temperature hydrogen and hydrocarbon sensors based on single nanowires of metal oxides, Journal of Physics D: Applied Physics, 2007, 40, 2777-2782.
6. Su L.M., Grote N., Schmitt F., Diffused planar InP bipolar transistor with a cadmium oxide film emitter, Electron. Lett., 1984, 20, 716-717.
7. Pianaro S.A., Bueno P.R., Olivi P., Longo E., Varela J.A., Effect of Bi₂O₃ addition on the microstructure and electrical properties of the SnO₂ .CoO.Nb₂O₅ varistor system, J. Mater. Sci. Lett., 1997, 16, 634-638.

8. Pianaro S.A., Bueno P.R., Longo E., Varela J.A., A new SnO_2 -based varistor system, *J. Mater. Sci. Lett.*, 1995, 14, 692-694.
9. Shinde S. D., Patil G. E., Kajale D. D., Ahire D. V., Gaikwad V. B., Jain G. H., Synthesis of ZnO nanorods by hydrothermal method for gas sensor applications, *International journal on smart sensing and intelligent systems*, 2012, 5, 57-70.
10. Castro M.S., Aldao C.M., Effects of thermal treatments on the conductance of tin oxide ,*J. Eur. Ceram. Soc.*, 2000, 20, 303-307.
11. Fayat J., Castro M.S., Defect profile and microstructural development in SnO_2 based varistor, *J. Eur. Ceram. Soc.*, 2003, 23, 1585-1591.
12. Lim Z.H., Chia Z.X., Kevin M., Wong A. S. W., Ho G.W., A facile approach towards ZnO nanorods conductive textile for room temperature multifunctional sensors, *Sensors and Actuators B*, 2010, 151, 121–126.
13. Wagh M.S., Jain G.H., Patil D.R., Patil S.A., L.A. Patil, Modified zinc oxide thick film resistors as NH_3 gas sensor, *Sensors and Actuators B*, 2006, 115,128-133.
14. Patil L.A., Shinde M.D., Bari A.R., Deo V.V., Patil D.M., Kaushik M.P., Fe_2O_3 modified thick films of nanostructured SnO_2 powder consisting of hollow microspheres synthesized from pyrolysis of ultrasonically atomized aerosol for LPG sensing, *Sensors and Actuators B*, 2011, 155, 174-182.
15. Cadena G., Riu J., Rius F., Gas sensors based on nanostructured materials, *Analyst*,2007, 132,1083-1099.
16. Prajapati C.S., Pandey S.N., Sahay P.P., Sensing of LPG with nanostructured zinc oxide thin films grown by spray pyrolysis technique, *Physica B*, 2011, 406, 2684.
17. Mardare D., Iacomi F., Cornei N., Girtan M., Luca D., Undoped and Cr-doped TiO_2 thin films obtained by spray pyrolysis, *Thin Solid Films*, 2010,518 4586-4589.
18. Wang Z., Hu Y., Wang W., Zhang X., Wang B., Tian H., Wang Y., Guan J., Gu H., Fast and highly-sensitive hydrogen sensing of Nb_2O_5 nanowires at room temperature, *Internatinal Journal of Hydrogen Energy*,2012,37, 4526–4532.
19. Patil L.A., Pathan I.G., Suryawanshi D.N., Bari A.R., Rane D.S., Spray pyrolyzed ZnSnO_3 nanostructured thin films for hydrogen Sensing, *Procedia Materials Science*, 2014, 6,1557 – 1565.
20. Parra R., Varela J.A., Aldao C.M., Castro M.S., Electrical and microstructural properties of (Zn, Nb, Fe)-doped SnO_2 varistor systems, *Ceramics International*, 2005, 31, 737-742.
21. Bari R.H., Khadayate R.S., Patil S.B., Bari A.R., Jain G.H., Patil L.A., Kale B.B., Preparation, characterization, and H_2S sensing performance of sprayed nanostructured SnO_2 thin films, *ISRN Nanotechnology*, 2012, ID 734325, 1-5.
22. Jain G.H., Patil L.A., Gaikwad V.B., Studies on gas sensing performance of $(\text{Ba}_{0.8}\text{Sr}_{0.2})(\text{Sn}_{0.8}\text{Ti}_{0.2})\text{O}_3$ thick film resistors *Sensors and Actuators B*, 2007,122,605-612.
23. Liu Huan, Wan Jiuxiao, Fu Qiuyun, Li Min, Luo Wei, Zheng Zhiping, Cao Hefeng, Hu Yunxiang, Zhou Dongxiang, Tin oxide films for nitrogen dioxide gas detection at low temperatures, *Sensors and Actuators B*, 2013, 177, 460-466.
24. Abbas M. N., Moustafa G.A, Gopel W., Multicomponent analysis of some environmentally important gases using semiconductor tin oxide sensors, *Analytica Chimica Acta*, 2001, 431, 181-194.
25. Su P.G., Jang W.R., Pei N. F., Detection of nitrogen dioxide using mixed tungsten oxide-based thick film semiconductor sensor, *Talanta*, 2003, 59, 667-672.
26. Ling Z., Leach C., The effect of relative humidity on the NO_2 sensitivity of a SnO_2/WO_3 heterojunction gas sensor *Sens & Act B*, 2004, 102, 102-106.
27. Ramgir N.S., Mulla I. S., Vijayamohanan K. P., A room temperature nitric oxide sensor actualized from Ru-doped SnO_2 nanowires, *Sens & Act B* 107 (2005) 708-715.
28. Rumyantseva M., Kovalenko V., Gaskov A., Makshina E., Yuschenko V., Ivanova I., Ponzoni A., Faglia G., Comini E., Nanocomposites $\text{SnO}_2/\text{Fe}_2\text{O}_3$: sensor and catalytic properties, *Sens & Act B*,2006, 118, 208-214.
29. Kaur J., Kumar R., Bhatnagar M.C., Effect of indium-doped SnO_2 nanoparticles on NO_2 gas sensing properties, *Sens & Act B*, 126 (2007) 478-484.
30. Hwang I.S., Kim S.J., Choi J.K., Choi H. Ji., Kim G.T., Cao G., Lee J. H., Synthesis and gas sensing characteristics of highly crystalline ZnO-SnO_2 core-shell nanowires, *Sens & Act B*,2010, 148, 595-600.
31. Bari R. H., Patil S. B., Bari A. R., Influence of precursor concentration solution on CO sensing performance of sprayed nanocrystalline SnO_2 thin films *Optoelectronics and advanced materials – rapid communications*, 2012,6, 887-895.
